Morphological, thermal and drug release studies of poly (methacrylic acid)-based molecularly imprinted polymer nanoparticles immobilized in electrospun poly (ε-caprolactone) nanofibers as dexamethasone delivery system

**Payam Zahedi[†], Mahshid Fallah-Darrehchi, Shima Ahmadi Nadoushan,
Robabeh Aeinehvand, Lida Bagheri, and Mohammad Najafi**

Nano-Biopolymers Research Laboratory, School of Chemical Engineering, College of Engineering,
University of Tehran, P. O. Box, 11155-4563, Tehran, Iran

Abstract−Electrospun poly (ε-caprolactone) (PCL) nanofibers containing molecularly imprinted polymer (MIP) nanoparticles based on methacrylic acid (MAA) were prepared for controlled release of dexamethasone (Dexa). First, the MIPs consisting of Dexa were synthesized via precipitation polymerization. Their recognition sites formation and thermal properties were investigated by FTIR and TGA tests, respectively. The results showed that by selecting a monomer: template (MAA : Dexa) molar ratio of 6 : 1, MIP nanoparticles were produced with imprinting factor of 1.80. The FESEM and TEM images showed the MIPs average diameter of 394±9.7 nm and appropriate immobilization of them in PCL nanofibers, respectively. Moreover, the cumulative release of Dexa from the MIP-loaded nanofibrous samples was studied by UV-vis spectrophotometry and revealed a suitable controlled release of the drug during four days. Afterward, Dexa release followed Higuchi model which indicated the main mechanism was governed by Fickian diffusion theory.

Keywords: Poly (ε-caprolactone), Molecular Imprinting, Nanofiber, Dexamethasone, Precipitation Polymerization, Drug Release

INTRODUCTION

One approach to palliate the host immune response is the synthesis of biomaterials along with controlled release of anti-inflammatory drugs. Among these drugs, dexamethasone (Dexa) is a well-known synthetic glucocorticoid that can effectively regulate the expression of inflammatory cytokines. In addition, Dexa is an active therapeutic drug for treating primary immune thrombocytopenia and perioperative immunosuppression of cardiac transplantation, preventing rejection of the transplanted organ, and preserving graft function [1-4]. However, Dexa has a short biological half-life of about 2-5 h in physiological environments, especially blood plasma, which remarkably decreases its efficiency during applying in the natural organs of the human body.

To increase the effectiveness of drugs like Dexa, which has low biological stability owing to its short half-life, some researchers have employed diverse particles and scaffolds made from polymeric materials [5-8]. The most significant goal of these synthetic polymeric carriers was omitting the initial burst release of drugs to provide systems that are capable to inject drugs with a long-term and controllable release due to keeping constant the effective dosage level of those drugs for higher performance.

Synthesis of nanoparticles based on Dexa has been abundantly attractive for increasing their positive effects. For these purposes, a wide variety of methods have been investigated, including emulsion polymerization [9,10], mini-emulsion polymerization [11,12], nanoprecipitation [13], and drug encapsulation into modified inorganic nanoparticles [14]. Among them, molecular imprinting a large number of functional monomers to provide a series of recognition active sites corresponding to a specific drug molecule is the conspicuous, practical and simple procedure. However, such efficient systems have not even been considered for Dexa while immobilizing the drug-loaded nanoparticles in electrospun polymeric nanofibers. Molecularly imprinted polymers (MIPs), owing to their small physical size, can provide widespread new functions which are out of access through bulk conditions. MIPs as smart micro- and nanoparticles imitate the structure of drug molecules by means of prepolymerization of functional monomers in the presence of template molecules [7,15-17]. Although the application of MIPs is apparently restricted to a drug delivery system (DDS), the preparation facility of this new class of materials has made them charismatic for extensive applications, such as chemical catalysis [18,19], chemical sensing [20,21], solid phase extraction [22,23] as well as chiral separation [24,25] and separation of toxic materials [26,27].

Besides MIPs, electrospun polymeric nanofibers containing different drugs are desirable candidates for DDS because of their unique properties, such as high aspect ratio. Interestingly, owing to the physical shape of nanofibers, they can be predominantly used in many internal or external medical applications compared to MIP nanoparticles. Biodegradable nanofibers such as poly (ε-caprolactone) (PCL) [5,8], poly (vinyl alcohol) (PVA) [28] and poly (lactic acid) (PLA) [29] used as Dexa nanocarriers have been considered for

[†]To whom correspondence should be addressed.
E-mail: phdzahedi@ut.ac.ir

controlled release applications. These studies showed that although polymeric nanofibers are suitable media, they cannot significantly prolong the drug release time more than overnight; as a result, after less than this time period, the appearance of a plateau trend in the drug release profile is inevitable [24]. To improve the drug release efficiency of nanofibers, encapsulating the MIP-based drugs into them can hopefully overcome this shortcoming, because the MIP nanoparticles are promising candidates for achieving a long-term controlled release of a wide range of drugs with respect to the nanofibers.

In the past few years, many drugs such as dipyridamole [30], citalopram [31], timolol maleate [32,33], gatifloxacin [34], glycyr-rhizic acid [35], tramadol [17], risperidone [12], prednisolone ace-tate [33] and nitroglycerine [36] have been employed as templates in the field of MIPs. The performance of synthesized MIPs in regard to their rebinding capacity and sustained control release of a specific drug deals with many factors. These parameters include the type and amounts of functional monomers and templates, the charac-teristics of crosslinking agents, porogenic solvents, initiators as well as time and temperature of polymerization. Recently, immobiliza-tion of MIP nanoparticles in electrospun nanofibers has attracted a great deal of attention due to the unique properties of nanofibers in terms of high specific surface area, low cost, and easy inclusion of nanoparticles through them.

Accordingly, Chronakis et al. [2] prepared MIP-based theophyl-line and 17β-estradiol nanoparticles within poly (ethylene tere-phthalate) (PET) nanofibers. They indicated that MIPs could be easily encapsulated into the polymer solution and designed a new type of recognition material that might utilize in separation, sens-ing and diagnostics applications. Zhang et al. [37] fabricated elec-trospun poly (acrylonitrile) (PAN) nanofibers containing p-nitro-phenol-imprinted nanoparticles. Their findings showed that the hydrolysis of paraoxon (diethyl-4-nitrophenyl phosphate) was 3.7-times higher than that of non-imprinted polymeric particles (NIPs). Also, the presence of electrospun PAN nanofibers could conve-niently separate the hydrolyzed paraoxon from a liquid phase.

Eventually, by following up the recent studies, we found that neither Dexa-loaded MIP nanoparticles directly nor encapsulat-ing them into polymeric nanofibers as a case study have been con-sidered. Therefore, our aim was to fabricate electrospun PCL nanofibers containing Dexa-loaded MIP nanoparticles based on poly(methacrylic acid) (PMAA) and then evaluate their morpho-logical, thermal and the drug release properties by using a series of different qualitative and quantitative tests.

MATERIALS AND METHODS

1. Materials

Methacrylic acid (MAA) (functional monomer, synthesis grade with purity of 98.5%), ethylene glycol dimethacrylate (EGDMA) (cross-linker, technical grade) and azobisisobutyronitrile (AIBN) (thermal initiator, a white powder with 98% purity) were purchased from Merck Co., Germany. First, MAA monomer was distilled under vacuum condition at 130 °C to remove its inhibitor and AIBN powder was recrystallized in methanol to increase its purity prior to precipitation polymerization. Dexamethasone (Dexa) (a white and crystalline powder, molecular weight of 392.5 g mol^{-1}, purity of 98% and a poorly-water soluble drug) and poly (ε-capro-lactone) (PCL) (biodegradable polymer, granulized with average molecular weight of 90 kg mol^{-1}) were provided from Sigma-Aldrich Co., The Netherlands. All the other chemicals were analytical reagent grades and used without further purification.

2. Synthesis of MIPs and NIPs Based on PMAA Nanoparticles

Table 1 shows the different formulations of MIP samples pro-duced by means of precipitation polymerization. As mentioned, MAA, Dexa, EGDMA, AIBN and acetonitrile were used as func-tional monomer, template, cross-linking agent, initiator and apolar porogenic solvent, respectively. Different molar ratios of MAA : Dexa (monomer: template) (2, 4, 6 and 8) were mixed into acetonitrile (40 mL in total volume) and stirred for 6 h. After the formation of complex, predetermined amounts of EGDMA (18 mmol or 754 μL) and AIBN (see Table 1) were added to the mixtures. Then, the mixtures were transferred to the glass containers, and prior to son-ication were degassed with purged nitrogen (N$_2$) for 15 min to com-pletely remove the moisture and oxygen from the reaction medium. Thereafter, the polymerization process was started in an oil bath at 60 °C for 24 h. In the last stage, the formed suspension solutions, including MIP nanoparticles, were centrifuged at 6,000 rpm, fil-tered and dried at room temperature. To remove the template, the dried synthesized nanoparticles were washed with a mixture of methanol : acetic acid (9 : 1) by means of a Soxhlet apparatus for 48 h. To prove that Dexa molecules were completely extracted from the MIP nanoparticles cavities, sampling from the supernatant was done after centrifuging to measure the Dexa amount by using a UV-vis spectrophotometry (model UVmini-1240, Shimadzu, Japan) at wavelength of 249 nm. On the other hand, the NIPs nanoparti-cles were synthesized similar to the procedure for MIPs produc-tion with this difference that the step of complex formation between the drug and monomer was eliminated. Thus, in the procedure of

Table 1. Different formulation of synthesized molecularly imprinted PMAA nanoparticles and their IF based on Dexa

Sample	MAA : Dexa (M : T) (molar ratio)	Dexa (T) (mmol)	MAA (M) (mmol)	EGDMA (C) (mmol)	AIBN (I) (mg)	IF
MIP$_2$	2 : 1	1	2	18	17	1.14
MIP$_4$	4 : 1	1	4	18	19	1.55
MIP$_6$	6 : 1	1	6	18	21	1.80
MIP$_8$	8 : 1	1	8	18	23	1.35

PMAA: poly (methacrylic acid), Dexa: dexamethasone, MIP: molecularly imprinted polymer, IF: imprinting factor, M: monomer, T: tem-plate, C: cross-linker, I: initiator, polymerization temperature=60 °C, polymerization time=24 h

NIPs synthesis, there was no Dexa template and therefore no cavities, including the active sites-miming the structure of the drug molecule were provided.

3. Electrospinning of PCL Solution Containing PMAA-based MIP Nanoparticles

In general, the MIP nanoparticles were suspended in a solvent mixture of chloroform : dimethylformamide (DMF) with ratio of 7 : 3 (v/v) by using sonication and then weighed PCL granules were dissolved in this suspension solution by stirring at ambient temperature for 2 h. The polymeric mixture containing MIP nanoparticles was sonicated again to attain a uniform dispersion of the nanoparticles in the polymeric solution with concentration of 9.5 (w/v). In this way, the mass ratio of MIPs : PCL was selected 1 : 25 (w/w). This amount was nearly equal to an effective dose of Dexa for inflammation therapy (0.4 mg mL^{-1}) [38]. The MIP-loaded PCL nanofibrous samples were prepared by utilizing an electrospinning device (model eSpinner-NF-COEN/II), Asian Nanostructures Technology Co., Iran. The optimized electrospinning conditions for the production of nanofibers were as follows: the solution flow rate 0.45 mL h^{-1}, the applied voltage 19.5 kV and the distance between the syringe needle tip and rotational collector 14.5 cm [28]. After the electrospinning process, the samples were removed from the collector and dried at room temperature for 12 h for further evaluations. The overall illustration of Dexa template-based MIP nanoparticles synthesis followed by their immobilization in electrospun PCL nanofibers is represented in Scheme 1.

4. Measurements

Regarding the batch rebinding experiments evaluate the drug loading capacity of the synthesized MIP and NIP nanoparticles, 75 mg of the washed samples was suspended in 20 mL of acetonitrile containing Dexa with concentration of 50 μg mL^{-1} and then the mixture was stirred for 4 h. Subsequently, the suspensions were centrifuged at 5,000 rpm for 15 min to separate the nanoparticles saturated with Dexa molecules from the solution. For statistical study, the binding experiments were repeated three times to calculate standard deviation (SD). The binding capacity, or in other words, the drug loading efficiency (Q), was defined as the amount (mg) of template bound per amount (mg) of nanoparticles according to Eq. (1):

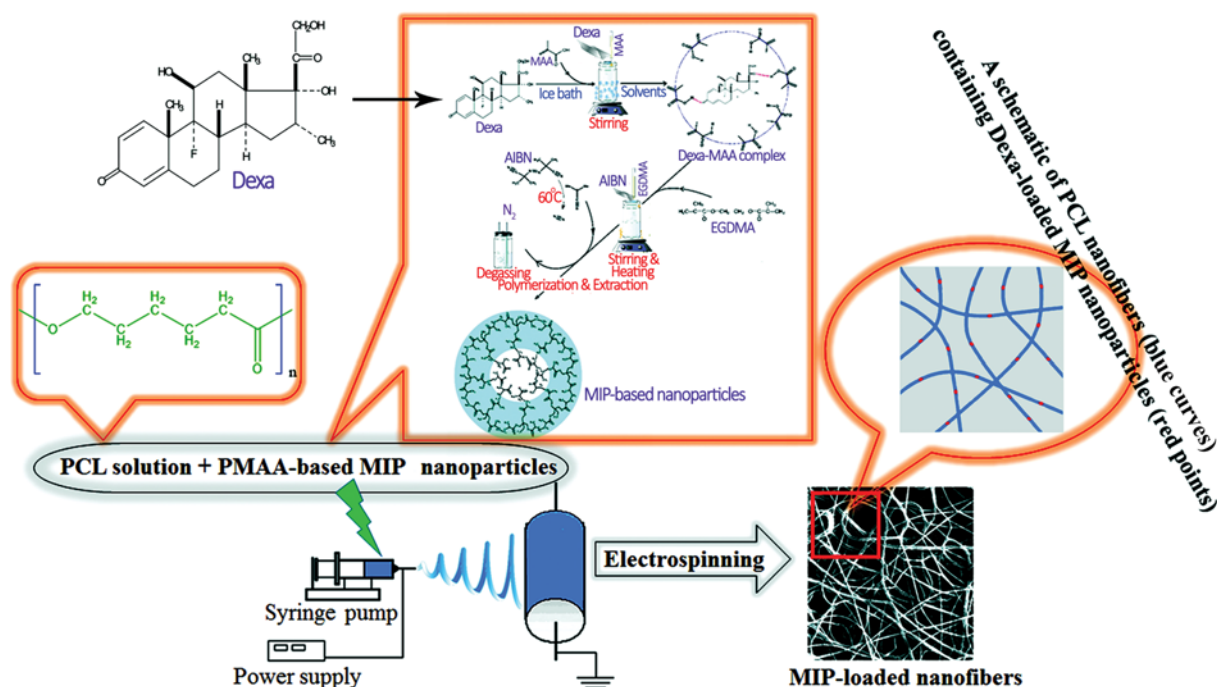$$\text{Binding capacity (Q)} = \frac{(C_0 - C) \times v}{w}, \tag{1}$$

where 'C_0' is the initial concentration, 'C' is the free concentration of Dexa in supernatant , 'v' (mL) is the volume of adsorption medium, and 'w' refers to the mass (mg) of nanoparticles. Moreover, imprinting factor (IF) as the main parameter in the molecular imprinting technique was calculated according to Eq. (2), below:

$$IF = \frac{Q_{MIP}}{Q_{NIP}}, \tag{2}$$

5. Characterization

For qualitative determination of the active sites formed through the MIP nanoparticles' cavities, Fourier transform infrared (FTIR) spectroscopy (model Spectrum Two, PerkinElmer Inc., United States) was utilized at room temperature with wavenumbers in a range of 400-4,000 cm^{-1} using a KBr tablet at a resolution of 4 cm^{-1}. This study was done for these samples before and after washing by the use of methanol : acetic acid with ratio of 9 : 1 (v/v).

The morphology observations of PMAA-based MIP nanoparticles and the nanoparticle-loaded electrospun PCL nanofibers were

Scheme 1. The overall schematic illustration of the preparation of Dexa-loaded MIP nanoparticles immobilized in electrospun PCL nanofibrous samples.

made with field emission scanning electron microscopy (FESEM) (model SU8040, Hitachi, Japan) at 60000 X magnification and an SEM (AIS 2100 model, Seron Technologies Inc., Korea) with 30000 X magnification, respectively. Prior to FESEM and SEM tests, all the samples were sputtered with a thin layer of gold using an auto sputter coater (model E5200, Bio-Rad, United Kingdom). By measuring at least ten different sections of the nanoparticles and nanofibers in the micrograph images, the average sizes along with their distribution curves of the samples were estimated by using ImageJ software.

To verify the presence of imprinted nanoparticles in MIP-incorporated PCL nanofibrous sample, transmission electron microscopy (TEM) (model CM30, JEOL, Japan) was utilized at an accelerating voltage of 100 kV at room temperature. To prepare the sample, the polymeric solution was electrospun on the copper grid for 15-20 seconds.

For investigation of the binding capacity of the MIP and NIP nanoparticles in regards to Dexa template as well as *in vitro* drug release studies of Dexa-loaded nanoparticles immobilized in electrospun PCL nanofibers immersed into PBS environment, UV-vis spectrophotometry with specification mentioned before was applied. To distinguish the amount of Dexa concentration in the release environment each time, the Dexa calibration curve was calculated according to Beer-Lambert law at maximum UV adsorption of the drug (λ_{max}=249 nm) [Eq. (3)]:

$$A=\varepsilon \times c \times l = 0.04095 \times c, \tag{3}$$

where 'ε' is the extinction coefficient of the drug solution, 'c' is the drug solution concentration and 'l' is the distance which the light travels through the sample (Usually it is equal to 1 cm). On the other hand, in regards to loading Dexa molecules within the MIP and NIP nanoparticles, after washing and drying them as far as no template has been detected, 75 mg of each sample was suspended in 20 mL of Dexa solution with concentration of 50 ppm and then sonicated for 12 min; subsequently, containers including the mixtures were shaken gently for 10 h. In continuous, the heterogeneous solutions were centrifuged at 5,000 rpm for 15 min; then the precipitated MIP and NIP nanoparticles were removed from the supernatant. By differentiating the Dexa concentration before and after the loading process, the amount of Dexa adsorption was measured by using the UV-vis spectrophotometer device and, therefore, the binding capacity percentage and IF of the samples was reported.

To assess the presence and absence of the template within the MIP nanoparticles' cavities and those NIPs surfaces as well as to compare the thermal stability behaviors between the washed and unwashed MIP nanoparticles samples, thermogravimetric analysis (TGA) (model TGA1, Mettler Toledo, Switzerland) was utilized. By considering initial weights around 12.1 mg for the three samples in terms of washed and unwashed MIP nanoparticles as well as the NIP samples, the weight loss percentages and their maximum rates at a specific degradation temperature were studied with TGA and derivative TGA (DTGA) curves, respectively. This experiment was carried out in temperature ranging from 25 °C to 500 °C at rate of 10 K/min under N_2 atmosphere with flow rate of 50 mL min^{-1}. Moreover, this test with the same conditions was applied for investigating the MIP nanoparticles remained within the electro-

spun PCL nanofibers before and after immersing into PBS to evaluate the nanoparticles residency within the nanofibers during the release assay.

In vitro drug release was done based on the following procedure: the electrospun nanofibers containing MIP and NIP nanoparticles incorporating the Dexa with concentration of 10 μg mL^{-1} were first weighed and then inserted into the dialysis bag made from cellulose acetate with 12 kDa cut-off. Then, these dialysis bags containing the nanofibers were immersed into the PBS (50 mL in total volume). To reach a uniform concentration of the released drug throughout the PBS environment, slight stirring was used during the process at room temperature. After each sampling from the supernatant, fresh PBS was added immediately to the containers to keep constant the total volume of release medium. Note that the water solubility of Dexa is about 89 mg L^{-1}; therefore, it can release through the aqueous medium, e.g., PBS during the drug release procedure. Eq. (4) shows the relationship between cumulative amounts of the released drug from the electrospun samples into PBS medium and release time.

$$\text{Cumulative release percentage: } \sum_{t=0}^{t} \frac{M_t}{M_0} \times 100 \tag{4}$$

where 'M$_t$' and 'M$_0$' are the cumulative amount of Dexa released at each sampling point and the initial amount of the drug loaded into the samples, respectively.

Furthermore, besides the Korsmeyer-Peppas equation four more models were studied to investigate the Dexa release mechanism from the PCL nanofibers in the presence and absence of MIPs. These models are well-known, the so-called zero-order, first-order, Higuchi and Hixon-Crowell. The selection of best model corresponding to the experimental release data depends on the calculated regression coefficient (R^2).

RESULTS AND DISCUSSION

1. Determination of a Suitable Monomer: Template Molar Ratio for MIP Nanoparticles

We considered different molar ratios of MAA : Dexa (monomer : template), whereas the other conditions in the precipitation polymerization for synthesizing the MIP nanoparticles were constant. By considering two main characteristics of MIP nanoparticles, such as binding capacity and morphology, the best monomer : template molar ratio was selected.

1-1. Binding Capacity

To recognize the optimum template/monomer molar ratio, the binding capacity percentages of Dexa onto the MIP and NIP nanoparticles were calculated based on Eq. (1). Table 2 indicates the obtained results for the samples with the monomer : template molar ratios of 2 : 1, 4 : 1, 6 : 1 and 8 : 1 denoted by MIP$_2$, MIP$_4$, MIP$_6$ and MIP$_8$, respectively (see Table 1). These results were also measured for NIP nanoparticles samples, noticeably they were synthesized in the absence of template. The obtained data proved that binding capacity percentage was directly dependent on monomer : template molar ratio. Thus, this value for 6 : 1 molar ratio of monomer : template, MIP$_6$ sample, was 61.7±1.2%, which referred to the most efficiency of this sample for Dexa adsorption. According

Table 2. The effect of template: monomer molar ratios on the binding capacity of Dexa onto MIPs and NIPs (mean±SD, n=3)

MAA : Dexa (molar ratio)	Binding of Dexa onto MIPs (%)	Binding of Dexa onto NIPs (%)
MIP_2 (2 : 1)	39.4±1.9	34.56±1.20
MIP_4 (4 : 1)	44.5±1.3	25.41±1.5
MIP_6 (6 : 1)	61.7±1.2	34.27±1.6
MIP_8 (8 : 1)	51.6±1.2	38.50±1.5

MIP: molecular imprinted polymer, NIP: non-molecular imprinted polymer, MAA: methacrylic acid monomer, Dexa: dexamethasone template
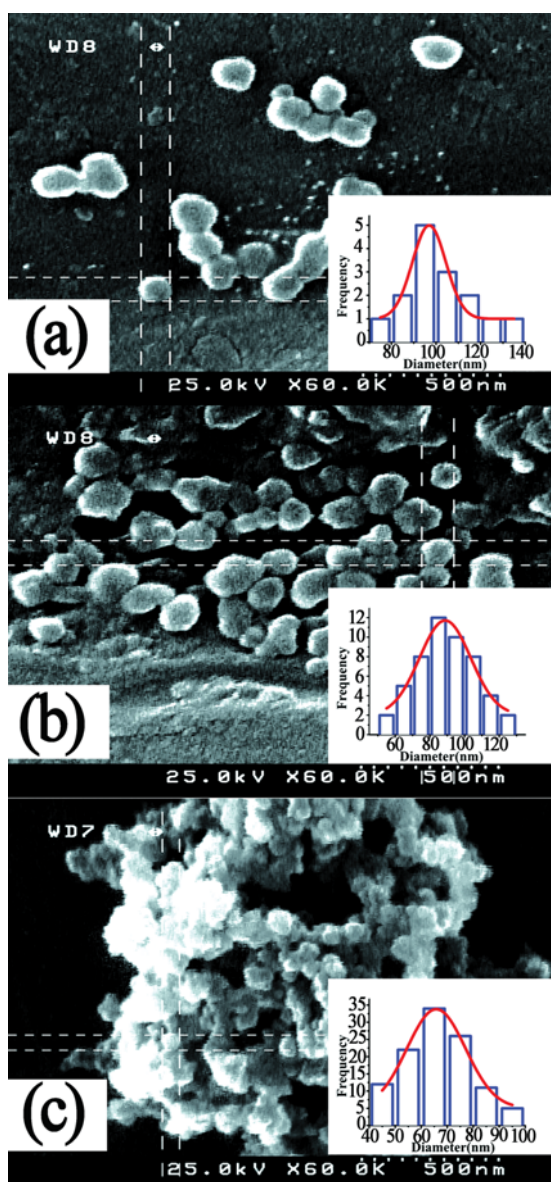

Fig. 1. FESEM micrograph images of MIP nanoparticles based on PMAA as a functional monomer and Dexa as a template along with EGDMA (cross-linker) and AIBN (initiator): (a) monomer : template molar ratio of 4 : 1, (b) monomer : template molar ratio of 6 : 1 and (c) monomer : template molar ratio of 8 : 1 (the scale bar is 0.5 microns).

to Eq. (2), the imprinting factors (IF) of MIP nanoparticles samples with mentioned different molar ratios were calculated and reported in Table 1. As is evident, MIP_6 sample with IF value of 1.80, based on Eq. (3) was selected as the best sample owing to formation of more active sites within its nanoparticles' cavities compared to another three samples.

1-2. Morphological Studies of the MIP Nanoparticle Samples

For further evaluation, the FESEM micrograph images of MIP_4, MIP_6 and MIP_8 nanoparticles samples are shown in Fig. 1(a)-(c). Also, the size distribution curve related to each sample is displayed in the right-hand side corner of the FESEM images. As can be seen from Fig. 1(a), although the morphology of MIP_4 nanoparticles was relatively suitable from the viewpoint of their sizes, the calculated IF based on binding capacity of the drug onto MIP_4 sample was not high enough (1.55). On the other hand, regarding Fig. 1(c), it exhibited the morphology of MIP_8 sample in which an agglomerated structure was clearly observed and that led to prevent the formed active sites through the cavities of MIP_8 nanoparticles; this phenomenon resulted in a low Dexa adsorption along with unacceptable IF (1.34). Fig. 1(b) shows the morphology of MIP_6 sample with well-dispersed nanoparticles as well as average diameter of 93±4.6 nm. Moreover, based on the binding capacity results, this sample has high tendency to adsorb the template molecules compared to the others. Therefore, MIP_6 nanoparticle sample was selected as the best one due to formation of ultra-fine particles and high IF, whereby it has been nominated as the efficient nanocarrier for further evaluations. The morphology of MIP_2 nanoparticles sample was not investigated because of its very low IF.

2. Recognition of the Active Sites in the Optimized MIP Samples

FTIR spectroscopy is a simple and appropriate tool to identify qualitatively the presence of those functional groups which have the indispensable role as active sites for adsorbing a specific molecule through MIP nanoparticles. However, the FTIR spectra of (a) NIP_6, (b) unwashed and (c) washed MIP_6 nanoparticles samples are shown in Fig. 2(a)-(c).
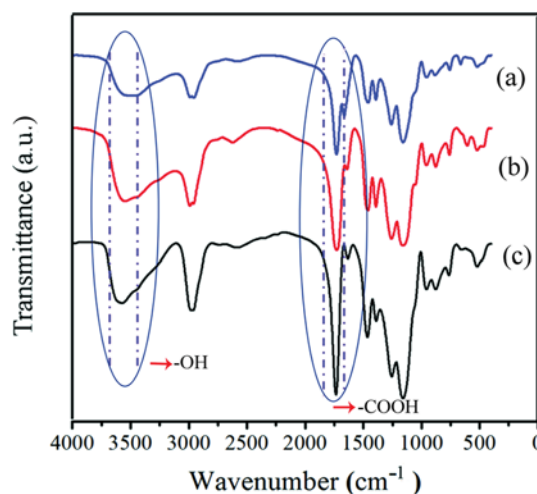

Fig. 2. FTIR spectra of PMAA-based nanoparticles: (a) NIP_6, (b) washed MIP_6 and (c) unwashed MIP_6. The washing solvents mixture was methanol : acetic acid (9 : 1 v/v).

As is obvious, two main characteristic peaks were observed; one peak was located at 3,509 cm^{-1} corresponding to hydroxyl groups (-OH), and another peak was seen at 1,729 cm^{-1} attributed to carboxyl groups (-COOH). The intensity of each peak was the main difference referring to the amount of functional groups within the NIP$_6$, unwashed and washed MIP$_6$ samples. The transmittance amount (the peaks intensity) confirmed that after removing Dexa with washing procedure, the intensity of hydroxyl and carboxyl groups, which provided active sites in the washed MIP$_6$ nanoparticles sample, was increased. Also, the results of some research works confirmed that the washing procedure intensifies the functional groups peaks [12,31,36]. The reason referred to the elimination of a series of non-covalent linkages between the drug and polymer, e.g., electrostatic, van der Waals and hydrogen bindings after the template removal. This occurrence resulted in the functional group amounts in the washed MIPs sample were increased owing to their formation when no linkage existed in the cavities. Overall, all the other FTIR characteristic peaks were the same in the NIP$_6$, unwashed and washed MIP$_6$ samples, attributed to PMAA backbone which was not changed during the washing process.

3. Thermal Stability of the Optimized MIP and NIP Nanoparticles

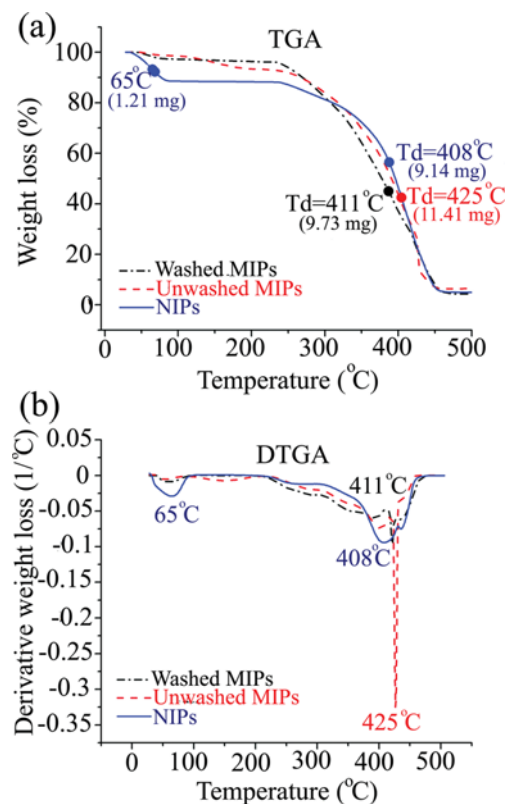Fig. 3(a), (b) demonstrates the weight loss percentages (TGA

Fig. 3. (a) TGA curves of washed MIP$_6$ nanoparticles (black dash point line), unwashed MIP$_6$ nanoparticles (red dash line) and NIP$_6$ nanoparticles (blue solid line); (b) derivative TGA (DTGA) curves of washed MIP$_6$ nanoparticles (black dash point line), unwashed MIP$_6$ nanoparticles (red dash line) and NIP$_6$ nanoparticles (blue solid line).

curves) and derivatives TGA curves of washed and unwashed MIP$_6$ samples as well as NIP$_6$ sample. By considering the TGA and DTGA curves of NIP$_6$ sample, two weight loss regions were observed at temperatures of 65 °C and 408 °C attributing to the evaporation of a little moisture e.g., methanol (1.21 mg) and amount of degraded Dexa (9.14 mg) onto the surface of this sample, respectively. An interesting result was obtained by comparing the thermal stability curves of washed and unwashed MIP samples. As can be seen from these curves, there was no weight loss region throughout the temperatures lower than 405 °C, which means purity of the samples without moisture. Owing to a large number of cavities formed within the MIPs structure, whole moisture was removed during the samples drying at room temperature. Also, in regards to unwashed MIP nanoparticles in which the template was entrapped through their cavities, a severe TGA peak in weight loss followed by a remarkable extremum in DTGA curves (red dash line) was observed. This trend was attributed to the Dexa molecules degradation along with diminishing MIP nanoparticles' active sites, which were linked to the template surface (the total weight loss of 11.41 mg). On the other hand, the washed MIP$_6$ showed no significant weight loss throughout the temperature increase; as a result, there was no template in this sample. The active sites formed within the sample's cavities were gradually degraded thermally in which a small peak in DTGA was observed. This was reasoned that the washed MIP$_6$ nanoparticles have the highest thermal stability compared to other samples. The pure weight loss related to the functional sites in washed MIP samples was around 9.73 mg. Finally, it can be concluded that the MIP$_6$ nanoparticles sample had no template after washing process and showed a slow thermal degradation (T_d=411 °C).

4. SEM and TEM Studies of Electrospun PCL Nanofibrous Samples in the Presence and Absence of MIPs and NIPs

Fig. 4(a)-(c) shows the SEM micrograph images of the samples including (a) PCL nanofibers containing MIP nanoparticles, (b) PCL nanofibers containing NIP nanoparticles and (c) Dexa-loaded electrospun PCL nanofibers. From Fig. 4(a), the addition of Dexa by means of optimized MIP$_6$ nanoparticles to PCL nanofibers led to almost more uniform and fine fibers with an average diameter of 394±9.7 nm. The obtained morphology from the drug loaded NIP-incorporated PCL nanofibers [Fig. 4(b)] demonstrates the nearly nonuniform fibers with broad average diameter distribution compared to MIP-loaded nanofibers, which are shown by Gaussian curves in the corner. By considering the MIP and NIP particle morphologies indicated below in Fig. 4(a) and (b), respectively, it could be concluded that non-uniformity in NIPs led to induce morphological irregularity. For example, a sudden increase in diameter size was observed, because NIP nanoparticles according to their image had agglomerated. Generally, the particle size of NIPs is smaller than MIPs, but owing to the surface activity of NIPs they tend to adhere to each other; as a result, some aggregates are formed which produce shapeless particles [39,40]. This trend resulted in the PCL nanofibers with a broad polydispersity compared to those samples containing MIPs. MAA-based NIPs are mostly smaller than MIPs, which confirmed our findings. Fig. 4(c) refers to the directly Dexa-loaded PCL nanofibers and exhibits the full of bead and non-uniform sample that was not susceptible to release the drug under the controlled conditions. The obtained results con-
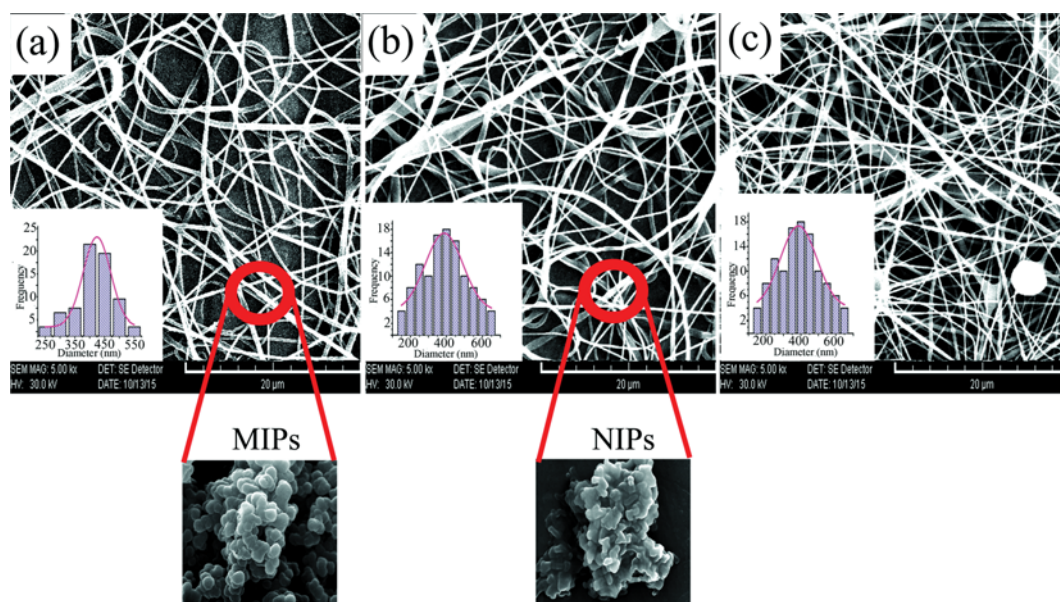
Fig. 4. SEM micrograph images of electrospun PCL nanofibers containing (a) Dexa-MIP$_6$ nanoparticles, (b) Dexa-NIP$_6$ nanoparticles and (c) Dexa directly (the scale bar is 20 microns).

firmed that the presence of Dexa in the shape of MIPs could produce better morphology in terms of diameter size and uniformity. In conclusion, the MIP-loaded PCL solution produced finer fibers. On the other hand, fulfillment of bead morphology of directly Dexa-loaded electrospun PCL nanofibers was observed because the Dexa role as a plasticizer into PCL chains resulted in a reduction in the polymer solution viscosity [41]. To confirm this claim, the viscosity of two different solutions, including PCL containing Dexa-loaded MIPs and Dexa, directly was measured and reported with the values of 0.25 and 0.18 Pa·s, respectively.

Fig. 5(a), (b) indicates the TEM images of neat and MIP-incorporated PCL nanofibers. As can be seen from Fig. 5(a), a smooth and uniform morphology of neat PCL nanofibers was observed. On the other hand, Fig. 5(b) demonstrates spherical bullet-like MIP nanoparticles in the length of nanofibers that proved the presence of MIPs within the nanofibers. In addition, the single spheres in Fig. 5(b) display the suitable dispersion and unwillingness of imprinted nanoparticles to migrate out of the fibers during the electrospinning process.
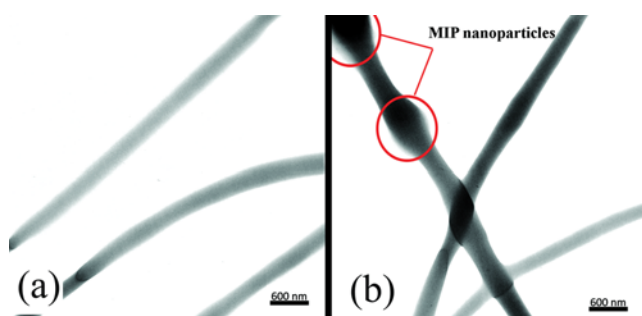

Fig. 5. TEM images of (a) neat PCL nanofibers and (b) MIP$_6$-incorporated PCL nanofibers (the scale bar is 0.6 micron).

5. *In Vitro* Drug Release from Electrospun PCL Nanofibers in the Presence and Absence of MIPs and NIPs

Besides the characterizations of synthesized MIP nanoparticles to choose the best template: monomer molar ratio, fabricating the PCL nanofibers containing optimized drug-loaded nanoparticles to have a sustained control release was the main goal. However, in this section, four different samples such as Dexa-loaded MIP$_6$ nanoparticles immobilized in electrospun PCL nanofibers, Dexa-loaded NIP$_6$ nanoparticles immobilized in electrospun PCL nanofibers, Dexa-loaded electrospun PCL nanofibers directly and Dexa-loaded MIP$_6$ nanoparticles samples were considered to study their drug
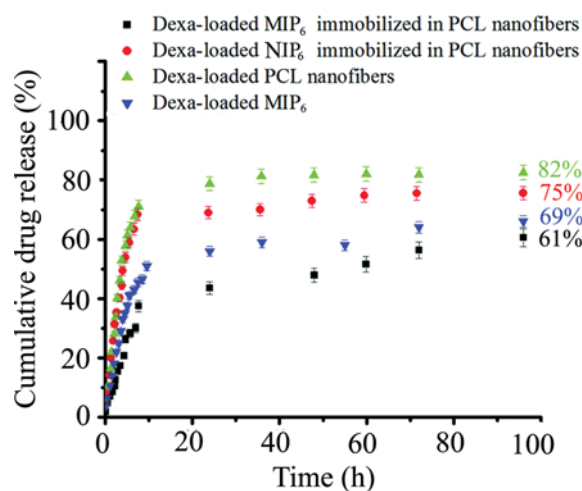

Fig. 6. Cumulative release profiles of Dexa-loaded MIP$_6$ immobilized in PCL nanofibers (■), Dexa-loaded NIP$_6$ immobilized in PCL nanofibers (●), Dexa-loaded PCL nanofibers (▲) and Dexa-loaded MIP$_6$ (▼) in PBS environment during 96 h time.

release as a function of time during four days. Fig. 6 depicts the Dexa release profiles of these four samples. Predictably, the Dexa-loaded electrospun PCL nanofibrous sample showed an initial burst release during 10 h, and then immediately a plateau level was observed until 96 h. It could be concluded that there were no drug molecules to exit from the nanofibrous samples and most of them (~80%) released after 10 h. To overcome this disadvantage, the NIP_6 and MIP_6 nanoparticles containing the drug with concentration of 10 μg mL^{-1} were added to the PCL nanofibers. The obtained results revealed that a sustained control release of both samples was achieved. Nevertheless, the NIP_6-immobilized in PCL nanofibers released the drug about 75% during first 24 h and then the remaining drug was diffused gradually out. By considering the MIP_6-immobilized in PCL nanofibers the initial burst release of Dexa was eliminated approximately as far as only the half of drug amounts was diffused out from the nanofibers until 10 h and the other drug was released with a gentle slope in the profile. The ultimate cumulative Dexa released from this sample was about 61% after four days. To confirm that the presence of PCL nanofibers could have a better performance in Dexa release with respect to the MIP_6 nanoparticles, the Dexa-loaded MIP_6 nanoparticles were also reported. As it is seen, PCL nanofibers could suitability prolong the Dexa release with a gentle slope in which the appearance of plateau stage was postponed until 96 h time period. It could be concluded that adding the Dexa-loaded MIP_6 nanoparticles immobilized in electrospun PCL nanofibrous sample was a promising nanocarrier for DDS. So, by releasing Dexa with a total of 61%, the level concentration of this drug in PBS was in the range of its effective dosage in which Dexa can act as an inflammatory drug in many biological applications [38].

For further investigation, five different models were studied on the release rate of Dexa from the MIP_6 immobilized in PCL nanofibrous samples. By the release data fitting on the basis of each model, the regression coefficient (R^2) values were calculated and reported in Table 3. It is obvious, Dexa release trend followed Korsmeyer-Peppas equation with R^2 value of 0.9103 in which the exponent amount 'n' was obtained 0.56. It means that Fickian diffusion mechanism was appropriate for the drug release in the samples. This result was also confirmed by studying the well-known release kinetic models, and the investigations showed that Higuchi was the best model corresponding to the experimental data.

6. The MIPs Consistency into PCL Nanofibers

To confirm the MIP_6 nanoparticle residency and their consistency through the PCL nanofibers during the release assay in the PBS environment, we focused on the amount of ash content of the
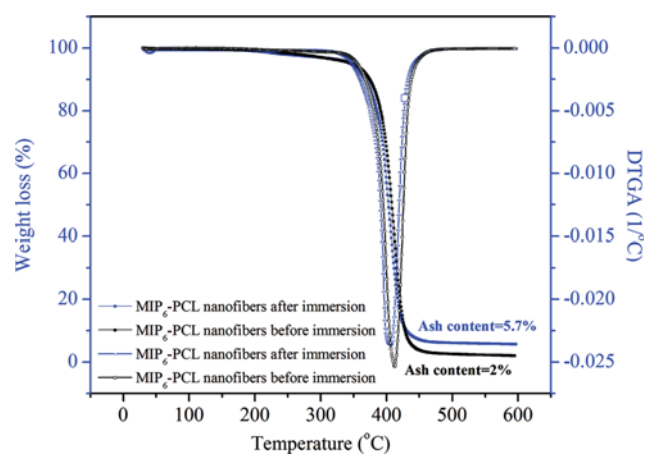
Table 3. Regression coefficients (R^2) based on different mathematical models for Dexa release from MIP_6 immobilized in PCL nanofibrous samples

Model	Equation	R^2
Zero-order	$Q_t = Q_0 + k_0 t$	0.2377
First-order	$\text{Ln } Q_t = \text{Ln } Q_0 + K_1 t$	0.4404
Higuchi	$Q_t = K_H \sqrt{t}$	0.8987
Hixon-Crowell	$Q_0^{1/3} - Q_t^{1/3} = K_s t$	0.3121
Korsmeyer-Peppas	$M_t / M_\infty = K_k t^n$, n=0.56	0.9103

Fig. 7. Ash content measurements of MIP_6-immobilized in PCL nanofibers before and after release test by using TGA curves.

samples before and after immersing them into PBS medium by using the TGA curves. Fig. 7 illustrates the weight loss of the samples in that a difference between the ash content of the samples before and after immersion was 3.7%. It emphasizes that a suitable portion of MIP_6 nanoparticles yet remained in the nanofibers.

CONCLUSIONS

We synthesized Dexa-loaded molecularly imprinted nanoparticles by using the precipitation polymerization so that in this way the suitable molar ratio of monomer : template was achieved (6 : 1). Also, the acceptable IF and ultrafine particles confirmed their suitability. Subsequently, Dexa-loaded MIP nanoparticles immobilized in PCL nanofibers were prepared under the appropriate electrospinning conditions. Besides the investigation of morphology and thermal behavior of those MIPs and NIPs samples, the fabrication of nanofibrous mats containing MIP nanoparticles for sustained control release of Dexa was the most significant objective. The SEM images showed that by incorporating the MIP nanoparticles into PCL solution, uniform and fine fibers were obtained. Moreover, the thermal trend of the optimized nanocarriers by using TGA test confirmed the stability of those washed MIP samples in exposure to high temperatures because of slower degradation rate during the heating procedure. TEM investigation proved the presence and acceptable dispersion of MIPs in the length of nanofibers. Furthermore, the release profile of Dexa revealed that MIP nanoparticles enabled to prolong the drug release time in the PCL nanofibrous samples. Additionally, the presence of MIP nanoparticles within the PCL nanofibers was proved by comparing the ash content of specimens before and after immersing them into PBS medium in the release assay.

COMPLIANCE WITH ETHICAL STANDARD

NOMENCLATURE

PCL   : poly (ε-caprolactone)
MIP   : molecularly imprinted polymer
Dexa   : dexamethasone
NIP   : non-imprinted polymer
PAN   : poly (acrylonitrile)
MAA   : methacrylic acid
PMAA   : poly (methacrylic acid)
EGDMA   : ethylene glycol dimethacrylate
AIBN   : Azobisisobutyronitrile
DMF   : Dimethylformamide
FTIR   : Fourier transform infrared
TGA   : Thermogravimetric analysis
DTGA   : Derivative thermogravimetric analysis
FE-SEM   : field emission scanning electron microscopy
SEM   : scanning electron microscopy
UV-vis   : Ultraviolet-visible
TEM   : Transmission electron microscopy
SD   : standard deviation
Q   : binding capacity
IF   : imprinting factor
M_t : cumulative amount of drug
M_0 : initial amount of drug
(v/v)   : (volume/volume)
(w/w)   : (weight/weight)

REFERENCES

1. D. H. Kim and D. C. Martin, *Biomaterials*, **27**, 3031 (2006).
2. I. S. Chronakis, A. Jakob, B. Hagstrom and L. Ye, *Langmuir*, **22**, 8960 (2006).
3. Q. Pan, Q. Xu, N. J. Boylan, N. W. Lamb, D. G. Emmert, J. C. Yang, L. Tang, T. Heflin, S. Alwadani and C. G. Eberhart, *J. Control. Release*, **201**, 32 (2015).
4. M. A. Kalam, *Int. J. Biol. Macromol.*, **89**, 559 (2016).
5. N. M. Vacanti, H. Cheng, P. S. Hill, J. D. T. Guerreiro, T. T. Dang, M. L. Ma, S. Watson, N. S. Hwang, R. Langer and D. G. Anderson, *Biomacromolecules*, **13**, 3031 (2012).
6. J. R. Li, R. Fu, L. Li, G. Yang, S. Ding, Z. D. Zhong and S. B. Zhou, *Pharm. Res.-Dordr.*, **31**, 1632 (2014).
7. W. M. Chen, D. W. Li, A. EI-Shanshory, M. El-Newehy, H. A. EI-Hamshary, S. S. Al-Deyab, C. L. He and X. M. Mo, *Colloid Surf. B-Biointerfaces*, **126**, 561 (2015).
8. Y. F. Li, M. Rubert, Y. Yu, F. Besenbacher and M. L. Chen, *Rsc Adv.*, **5**, 34166 (2015).
9. C. Giovannoli, C. Passini, L. Anfossi, F. D. Nardo, G. Spano, V. Maurino and C. Baggiani, *J. Sep. Sci.*, **38**, 3661 (2015).
10. K. Takimoto, E. Takano, Y. Kitayama and T. Takeuchi, *Langmuir*, **31**, 4981 (2015).
11. M. Pourfarzib, M. Shekarchi, H. Rastegar, B. Akbari-Adergani, A. Mehramizi and R. Dinarvand, *J. Chromatogr. B*, **974**, 1 (2015).
12. E. Asadi, S. Azodi-Deilami, M. Abdouss, D. Kordestani, A. Rahimi and S. Asadi, *Korean J. Chem. Eng.*, **31**, 1028 (2014).
13. Y. F. Shi, H. L. Lv, X. F. Lu, Y. X. Huang, Y. Zhang and W. Xue, *J. Mater. Chem.*, **22**, 3889 (2012).
14. Q. Gan, J. Zhu, Y. Yuan, H. Liu, J. Qian, Y. Li and C. Liu, *J. Mater. Chem. B*, **3**, 2056 (2015).
15. B. Sellergren and A. J. Hall, Molecularly imprinted polymers: From molecules to nanomaterials, John Wiley & Sons Ltd., New York (2012).
16. L. Ye and K. Mosbach, *Chem. Mat.*, **20**, 859 (2008).
17. M. Javanbakht, A. M. Attaran, M. H. Namjumanesh, M. Esfandyari-Manesh and B. Akbari-Adergani, *J. Chromatogr. B*, **878**, 1700 (2010).
18. G. Wulff, *Chem. Rev.*, **102**, 1 (2002).
19. F. Mirata and M. Resmini, Molecularly imprinted polymers in biotechnology, Springer, Heidelberg (2015).
20. K. Haupt and K. Mosbach, *Chem. Rev.*, **100**, 2495 (2000).
21. E. Mazzotta, A. Turco, I. Chianella, A. Guerreiro, S. A. Piletsky and C. Malitesta, *Sensor. Actuat. B-Chem.*, **229**, 174 (2016).
22. E. Turiel, M. Díaz-Álvarez and A. Martín-Esteban, *J. Chromatogr. A*, **1432**, 1 (2016).
23. X. Su, X. Li, J. Li, M. Liu, F. Lei, X. Tan, P. Li and W. Luo, *Food Chem.*, **171**, 292 (2015).
24. M. Kempe, K. Mosbach and L. Fischer, *J. Mol. Recognit.*, **6**, 25 (1993).
25. J. Yin, G. Yang and Y. Chen, *J. Chromatogr. A*, **1090**, 68 (2005).
26. Y. Yang, X. Liu, M. Guo, S. Li, W. Liu and B. Xu, *Colloid Surface A*, **377**, 379 (2011).
27. E. Caro, R. M. Marcé, P. A. G. Cormack, D. C. Sherrington and F. Borrull, *J. Chromatogr. A*, **1047**, 175 (2004).
28. P. Zahedi, I. Rezaeian, S. H. Jafari and Z. Karami, *Macromol. Res.*, **21**, 649 (2013).
29. L. T. H. Nguyen, S. Liao, C. K. Chan and S. Ramakrishna, *J. Biomat. Sci.-Polym. E.*, **23**, 1771 (2012).
30. M. Esfandyari-Manesh, M. Javanbakht, F. Atyabi, A. Mohammadi, S. Mohammadi, B. Akbari-Adergani and R. Dinarvand, *Mat. Sci. Eng. C-Mater.*, **31**, 1692 (2011).
31. M. Abdouss, E. Asadi, S. Azodi-Deilami, N. Beik-mohammadi and S. A. Aslanzadeh, *J. Mater. Sci.-Mater. M.*, **22**, 2273 (2011).
32. H. Hiratani, A. Fujiwara, Y. Tamiya, Y. Mizutani and C. Alvarez-Lorenzo, *Biomaterials*, **26**, 1293 (2005).
33. B. Malaekeh-Nikouei, F. A. Ghaeni, V. S. Motamedshariaty and S. A. Mohajeri, *J. Appl. Polym. Sci.*, **126**, 387 (2012).
34. X. F. Lu, Y. F. Shi, H. L. Lv, Y. Y. Fu, D. Ma and W. Xue, *J. Mater. Sci.-Mater. M.*, **25**, 1461 (2014).
35. G. Cirillo, M. Curcio, O. I. Parisi, F. Puoci, F. Iemma, U. G. Spizzirri, D. Restuccia and N. Picci, *Food Chem.*, **125**, 1058 (2011).
36. A. Mohebali, M. Abdouss, S. Mazinani and P. Zahedi, *Polym. Adv. Technol.*, **27**, 1164 (2016).
37. L. Zhang, Y. Guo, W. H. Chi, H. G. Shi, H. Q. Ren and T. Y. Guo, *Chin. J. Polym. Sci.*, **32**, 1469 (2014).
38. T. Hickey, D. Kreutzer, D. J. Burgess and F. Moussy, *J. Biomed. Mater. Res.*, **61**, 180 (2002).
39. C. Miura, H. Matsunaga and J. Haginaka, *J. Pharmaceut. Biomed.*, **127**, 32 (2016).
40. Y. Nakamura, H. Matsunaga and J. Haginaka, *J. Sep. Sci.*, **39**, 1542 (2016).
41. M. Zamani, M. Morshed, J. Varshosaz and M. Jannesari, *Eur. J. Pharm. Biopharm.*, **75**, 179 (2010).